



4th IASPEI / IAEE International Symposium:

Effects of Surface Geology on Seismic Motion

August 23–26, 2011 • University of California Santa Barbara

TUNING THE DEEP VELOCITY STRUCTURE MODEL OF THE TOKYO METROPOLITAN AREA BASED ON 1-D SIMULATION OF LONG-PERIOD S-WAVES

Yadab Prasad Dhakal
Tokyo Institute of Technology
Yokohama, 226-8502
Japan

Hiroaki Yamanaka
Tokyo Institute of Technology
Yokohama, 226-8502
Japan

Tsutomu Sasatani
Hokkaido University
Sapporo, 060-8628
Japan

ABSTRACT

Yamanaka and Yamada (2006) reconstructed the 3-D velocity structure model of the Kanto basin based on the Rayleigh wave phase velocities at periods from 0.5 to 5 s derived from the microtremor array observations at more than 300 sites in the area. In this paper, we perform 1-D simulation of long-period S-waves at sites in the north-west region of the Kanto basin for nearby, moderate magnitude, intermediate-depth earthquakes using their model. Based on the S-waveform comparisons, we find that the Yamanaka and Yamada model reproduces well the observed S-waveforms at most sites located in the Tokyo metropolitan areas. However, some of the sites near the basin edges need refinement of the velocity structure. Second, we tune the 1-D velocity structure beneath those sites so as to reproduce the observed S-waves from several earthquakes using the 1-D simulation; in doing so, we keep the velocity of each layer same to that in the base model but adjust the thickness of the sedimentary layers. We, therefore, aim to reconstruct an improved 3-D velocity structure model combining the modified 1-D structures with the existing 3-D model.

INTRODUCTION

Many big cities with a large population and long-period structures such as high-rise buildings and large oil-storage tanks, which are susceptible to long-period ground motions, are located today on the deep sedimentary basins. The 3-D velocity structure of the sedimentary basins greatly controls the amplitude and duration of long-period ground motions during large earthquakes. Many institutes are involved in constructing and updating the 3-D velocity structure models of the deep sedimentary basins for the seismic disaster mitigation planning in Japan (e.g., Koketsu *et al.*, 2008). As a result, several 3-D velocity models have been proposed for the Kanto basin, which is the largest basin in Japan. Although the objective of constructing such models is to accurately predict the long-period ground motions, the models are different because they have been constructed using different data sets such as geophysical (Koketsu and Higashi, 1992), geological (Suzuki, 1999), and earthquake data (e.g., Suzuki and Yamanaka, 2009). Therefore, joint inversion methods have been also applied to reconstruct integrated velocity model of the Kanto basin using the different data sets (e.g., Afnimar *et al.*, 2003; Tanaka *et al.*, 2005; Suzuki and Yamanaka, 2010).

Yamanaka and Yamada (2006) reconstructed the 3-D velocity structure model of the Kanto basin based on the Rayleigh wave phase velocities at periods from 0.5 to 5 s deduced from the microtremor array observations at more than 300 sites in the area. One of the advantages of using the deep sedimentary models from microtremor survey method for the simulation of long-period ground motions is that the models by this method are based on the principle of propagation of long-period surface waves in the sedimentary plains, where the surface waves are dominant for longer durations during large earthquakes. In this paper, we, therefore, consider the Yamanaka and Yamada (2006) model as a base model for tuning the deep S-wave velocity structure of the north-west region of the Kanto-basin. The strong motion observation sites and epicenters of the earthquakes used in this study are depicted in Fig. 1.

EARTHQUAKES USED

We selected four nearby earthquakes having magnitude M_w 5.2~ 5.9 and focal depth of 68 ~101 km. We used the hypocenter location determined by Japan Meteorological Agency (JMA) except for Event No. 2 in Table 2. The focal mechanism and epicentral location of the events are shown in Fig. 1. We used the centroid location, focal mechanism, and seismic moment determined by the Global CMT project for the Event No. 2 because the Global CMT solution produced a better fit between the observed and synthetic S-waves at rock sites near the target area. For other events, the focal mechanism and seismic moment are taken from the F-net moment tensor solution. We assumed a point source model for each earthquake and derived a triangle shaped source time function of duration ranging from 0.9 to 1.85 s by reproducing the observed S-waves at stiff soil and rock sites. The earthquake source parameters used in this study are summarized in Table 2.

Table 1. Material parameters of the velocity structure model used in this study

Layer	Vp (km/s)	Vs (km/s)	Density (g/cm ³)	Depth (top of layer) (km)	Qp and Qs
1	1.69-2.19	0.30~0.80	1.78~2.01	0.00	100
2	2.40	1.00	2.10	<i>variable</i>	100
3	3.20	1.50	2.25	<i>variable</i>	150
4	5.60	3.00	2.50	<i>variable</i>	300
5	6.00	3.30	2.70	5.00	500
6	6.80	3.74	2.90	14.00	600
7	7.60	4.18	3.20	27.00	1000
8	8.10	4.50	3.40	60.00	1000
9	8.30	4.57	3.50	70.00	1000

Table 2. Earthquake source parameters used in this study

Event No.	Date and Time (JST)	Strike (°)	Dip (°)	Rake (°)	Depth (km)	Rise time (s)	Mo (dyne.cm) ($\times 10^{23}$)
1	1997/09/08 08:40	50	71	41	101.0	0.9	6.62
2	2006/02/01 20:36	232	72	-6	101.0	0.9	5.07
3	2004/10/06 23:40	200	31	107	70.5	1.3	47.8
4	2005/07/23 16:35	165	28	69	68.0	1.85	91.1

1-D SIMULATION

We perform the 1-D simulation of long-period S-waves using the earthquake source parameters and the velocity structure model described in the previous sections. We apply the discrete wavenumber method (Bouchon, 1981) for the waveform simulation. Because of the limited space, we show a comparison of the S-waveforms for only the horizontal components at selected sites which are common to the used three or all four earthquakes. In the comparison, we focus on the first cycle of the observed and synthetic S-waveforms.

1997/09/08 Earthquake (Event No. 1, Table 2)

Figure 3 displays the bandpass filtered [0.25 to 0.5 Hz] observed and synthetic S-waveforms for the 1997 event. The waveforms are plotted in order of epicentral distance. The observed S-waveforms are well reproduced at the IBR005 and TCG011 sites, which are located on stiff soils above the shallow seismic basement (see Fig. 2). The first cycle of the observed S-waveforms exhibits a good agreement with the synthetic S-waveforms at the following deep soil sites: TKY007, IBR016, TKY006, SIT003, and GNM010. The synthetic S-waveforms underestimate the observed ones at the deep soil CHB002 and CHB001 sites, while they overestimate at the TCG012 and SIT001 sites, suggesting an inappropriate velocity structure beneath the sites.

Figure 4 displays the bandpass filtered [0.15 to 0.5 Hz] observed and synthetic S-waveforms for the 2006 event. The waveforms are plotted in order of epicentral distance. The observed S-waveforms are well reproduced at the TCG011 site, which is located on stiff soil above the shallow seismic basement (see Fig. 2). The observed S-waveforms at the CHB002, TKY026, IBR016, TKY015, SIT003, and GNM010 deep soil sites are also well reproduced. At the TCG012 site, the observed S-waveforms are overestimated similar to the previous event. At the other sites, one of the two horizontal components shows a good agreement between the observed and synthetic S-waveforms while the other component either underestimates or overestimates the observed one. In fact, some of these sites, such as the TKY007 and TKY006 sites, showed good agreements between the observed and synthetic S-waveforms for the both components for the previous event.

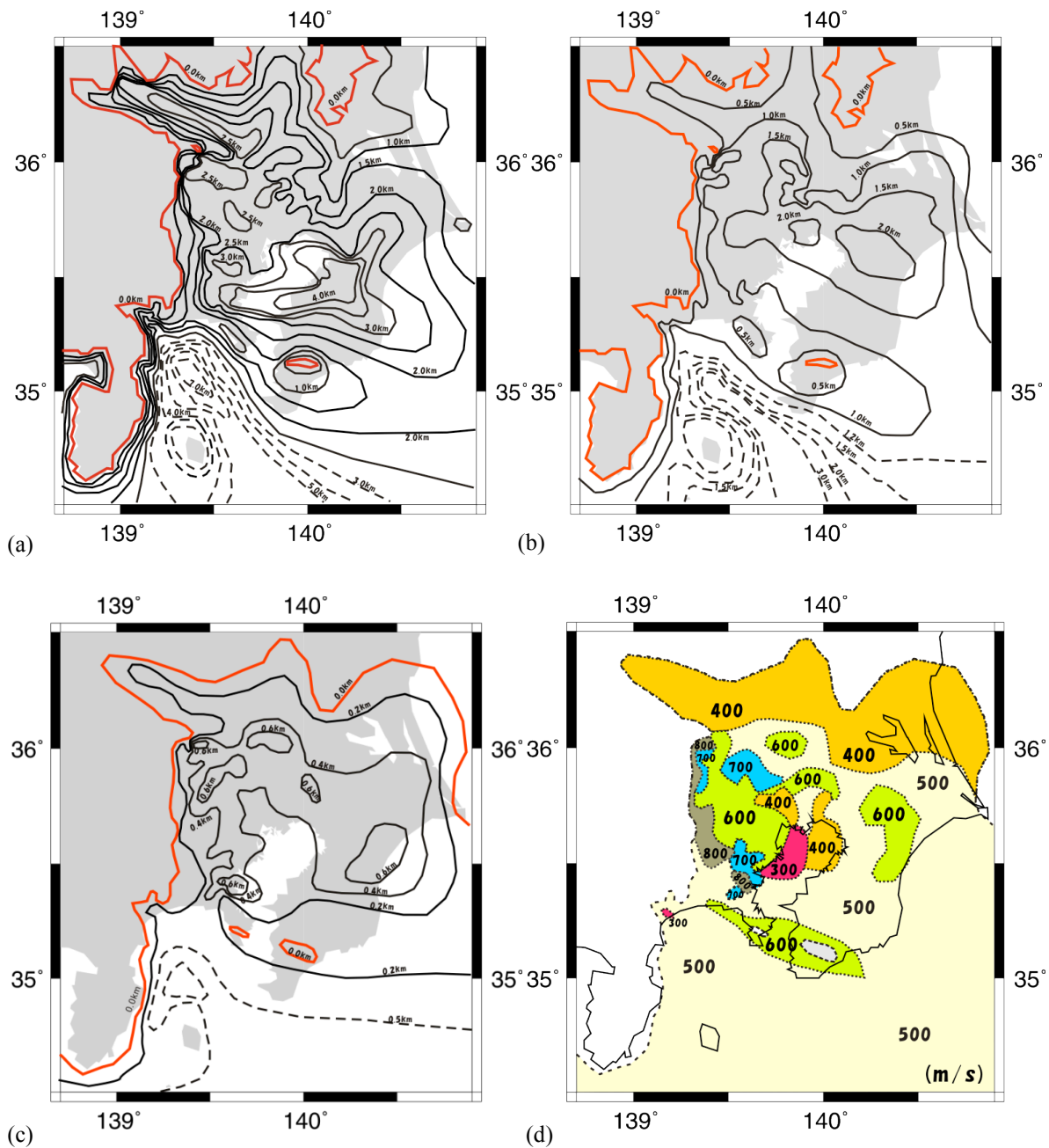


Fig. 2. Maps showing the depths to the top of layers having S-wave velocities of (a) 3.0, (b) 1.5, and (c) 1.0 km/s with variation of (d) S-wave velocity of the top layer in m/s (after Yamanaka and Yamada, 2006). The contours of 0 m depths for the layers in (a), (b), and (c) are indicated by red lines.

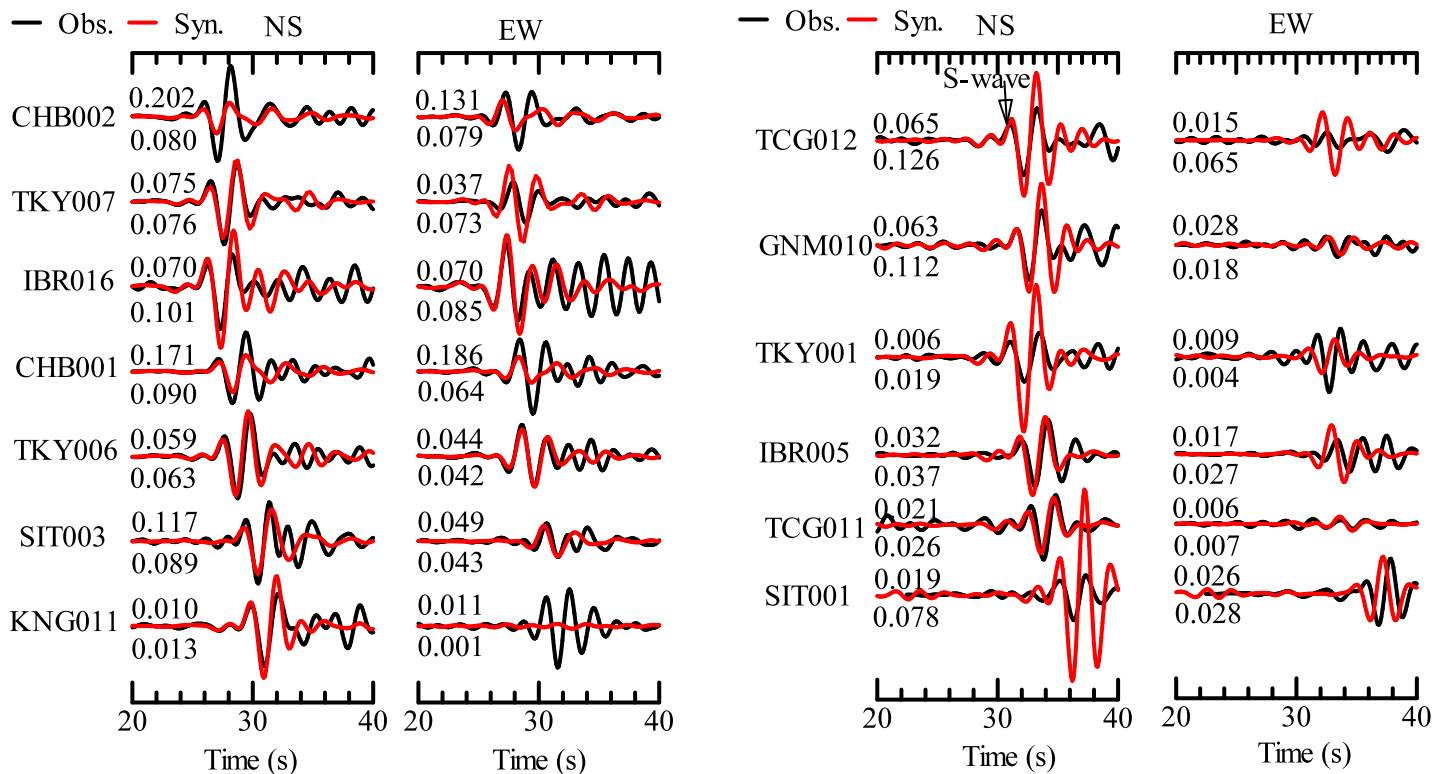


Fig. 3. Observed (black) and synthetic (red) velocity waveforms for the Mw 5.2, 1997 earthquake (Event No. 1, Table 2). The waveforms are bandpass filtered at 0.25-0.5 Hz; they are normalized by the maximum observed S-wave amplitude at each site. Numbers attached above and below to each waveform show the maximum amplitudes in cm/s for the observed and synthetic S-waveforms, respectively. The waveforms are plotted in order of epicentral distance and the site codes are indicated at the left of the NS component waveforms.

2004/10/06 Earthquake (Event No. 3, Table 2)

The bandpass [0.1-0.5 Hz] filtered observed and synthetic S-waveforms for the 2004 event are displayed in Fig. 5. The waveforms are plotted in order of epicentral distance. The observed and synthetic S-waveforms show very good agreement at the IBR005 and TCG011 sites, which are located on stiff soils above the shallow seismic basement (see Fig. 2). Similar to the previous two events, the observed S-waveforms are well reproduced at the deep soil site, IBR016. Also, the observed S-waveforms are reasonably well reproduced at the CHB002, TKY015, TKY026, SIT003, and TKY007 deep soil sites. Different from the previous two events, the synthetic S-waveforms show a good agreement with the observed ones on the large amplitude EW component at the CHB001 site and underestimate at the GNM010 site. But similar to the previous two events, the synthetic S-waveforms overestimate the observed ones at the TCG012 site. At the other sites mostly located in the western part of the basin, the S-waveforms are systematically overestimated on the EW components. This is directly related to the radiation pattern effect of the S-waves as discussed in the last section of this paper.

2005/07/23 Earthquake (Event No. 4, Table 2)

The bandpass [0.1-0.5 Hz] filtered observed and synthetic S-waveforms for the 2005 event, which is the largest magnitude event (Mw 5.9) among the used four earthquakes, are displayed in Fig. 6. The waveforms are plotted in order of epicentral distance. The observed and synthetic S-waveforms show a good agreement at the IBR005, TCG011, and TKY001 sites, which are located on stiff soils above the shallow seismic basement (see Fig. 2). Similar to the previous three events, the observed S-waveforms are well reproduced at the deep soil site, IBR016. Also, the observed S-waveforms are reasonably well reproduced at the TKY026, CHB002, TKY015, TKY007, CHB001, TKY006, SIT003, SIT009, and SIT002 deep soil sites. Keeping the track of previous three events, the synthetic S-waveforms overestimate the observed ones at the TCG012 site for this event also. The synthetic S-waveforms at the GNM010 and SIT001 strongly underestimate the observed ones on the EW and NS components, respectively, suggesting further investigations on

the used velocity structure.

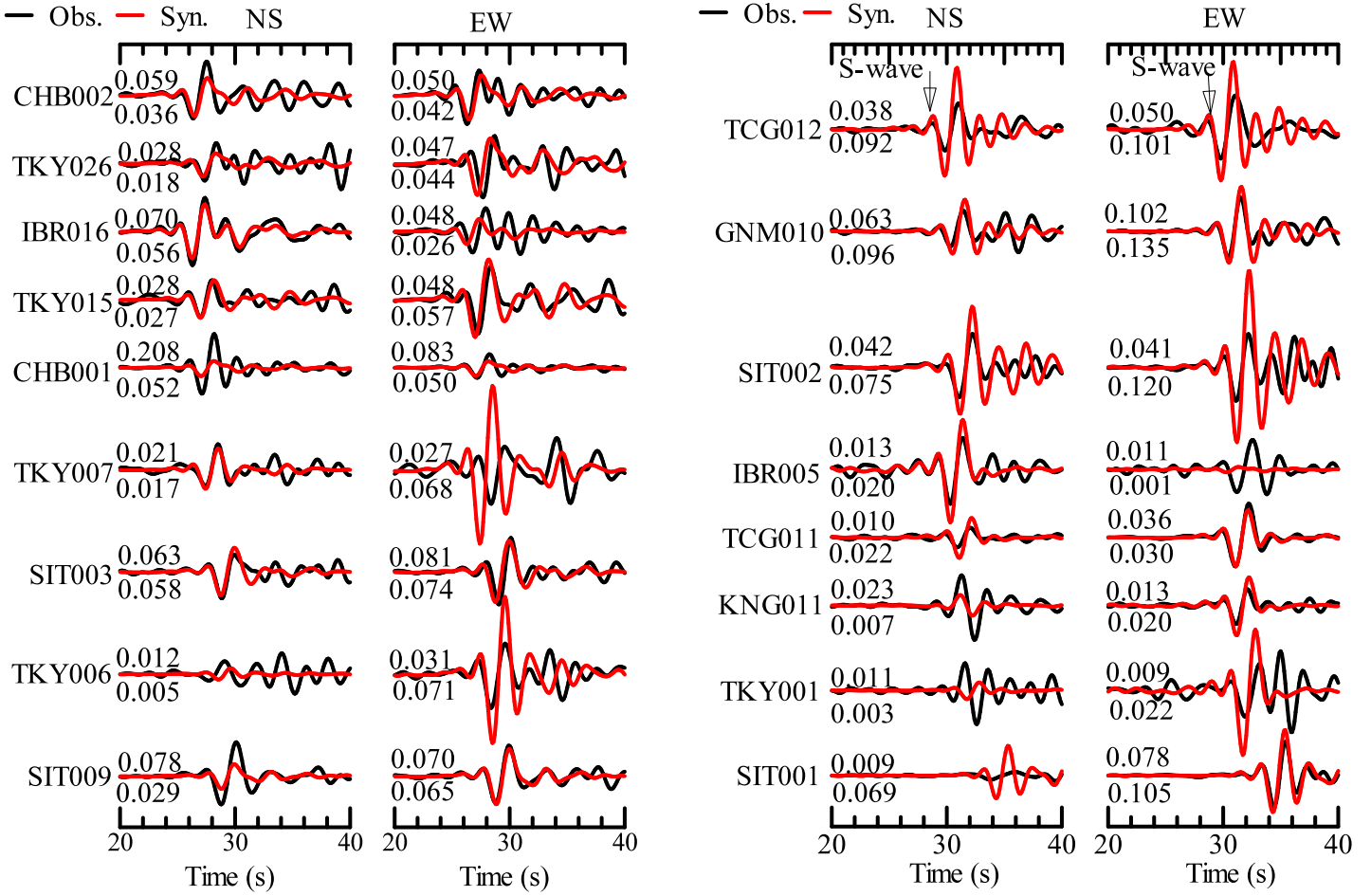


Fig. 4. Observed (black) and synthetic (red) velocity waveforms for the Mw 5.2, 2006 earthquake (Event No. 2, Table 2). The waveforms are bandpass filtered at 0.15-0.5 Hz; they are normalized by the maximum observed S-wave amplitude at each site. See captions in Fig. 3 for other details.

TUNING

In the previous section, we found that the synthetic S-waveforms systematically overestimated the observed S-waveforms at the TCG012 site for the all used earthquakes. We noted that the radiation pattern of S-wave has strong effect on the amplitude of the S-waveforms. However, the good agreement between the observed and synthetic S-waveforms at the nearby TCG011 and IBR005 stiff soil sites indicate that the used source parameters are satisfactory to apply for tuning the deep velocity structure at the TCG012 site.

Here we select a series of bandpass filters to compare the observed and synthetic S-waveforms starting from the low frequency band based on the theoretical site amplifications. We assume that the number of sedimentary layers and the velocity of each layer are the same as those in the base model. Then we change the thickness of the sedimentary layers on a trial basis until the observed and synthetic S-waveforms fit well for the low frequency band. We check whether the new structure explains the observed S-waveforms for the higher band than the previous ones. We try to keep the site amplifications that reproduced the observed S-waveforms for the previous band and adjust the velocity structure to reproduce the observed S-waveforms for the higher frequency band. We continue the process until the observed S-waveforms are well reproduced for the several frequency bands. In doing so, we compare only the first cycle of the S-waveforms in the time domain and the Fourier spectra in the frequency domain; the time window for spectral analysis is about 10s setting the first cycle of the S-waveforms at the centre of the time window (Dhakal *et al.*, 2009).

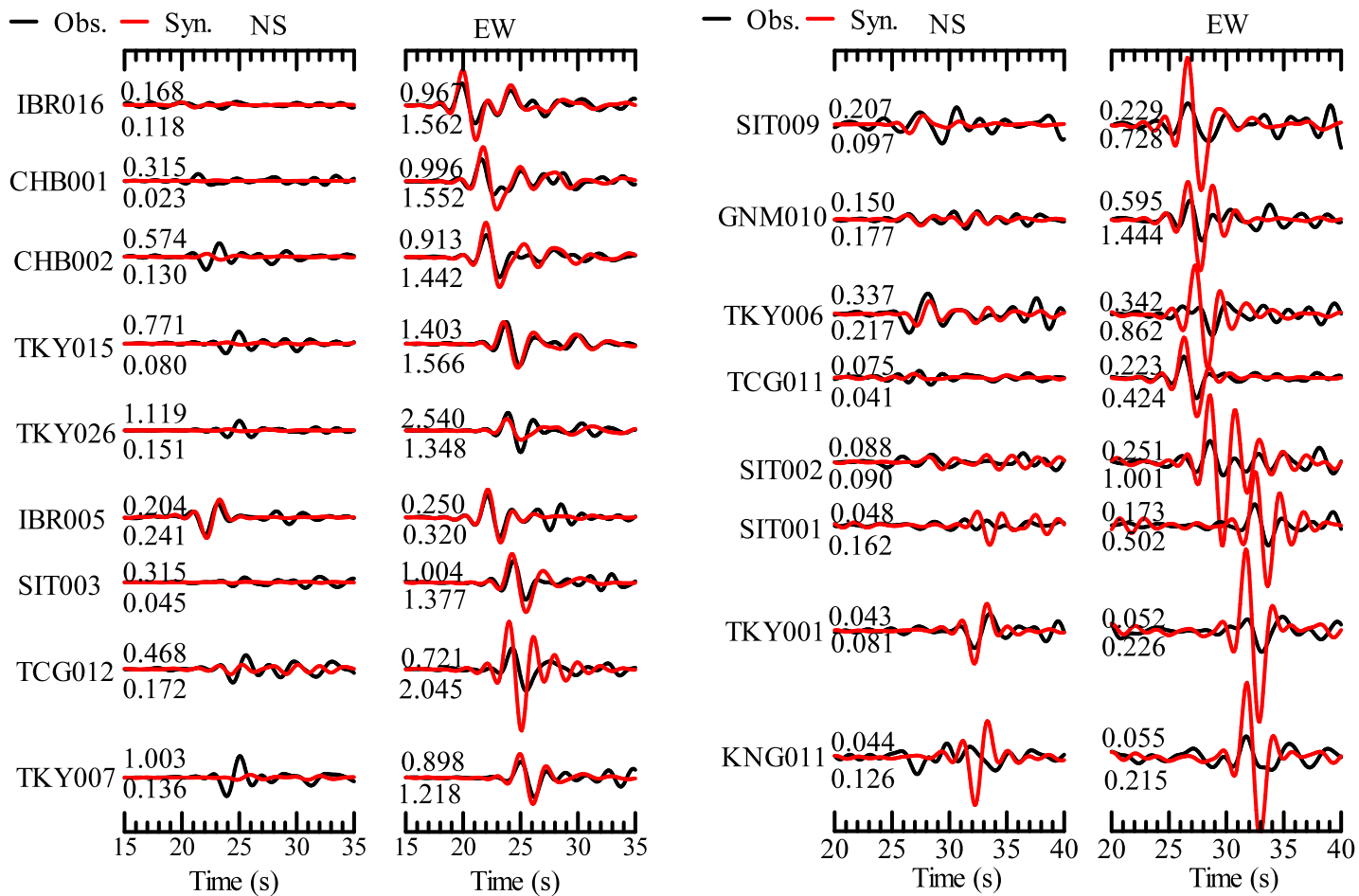


Fig. 5. Observed (black) and synthetic (red) velocity waveforms for the Mw 5.7, 2004 earthquake (Event No. 3, Table 2). The waveforms are bandpass filtered at 0.1-0.5 Hz; they are normalized by the maximum observed S-wave amplitude at each site. See captions in Fig. 3 for other details.

Figure 7 displays the observed S-waveforms and the synthetic ones for the tuned and original structures at the TCG012 site for the four earthquakes used in this study. In the figure, we can see that for all earthquakes the synthetic S-waves using the original model strongly overestimates the observed S-waves for all frequency bands. On the other hand, the tuned structure reproduces the observed S-waves well for all frequency bands for the all four earthquakes. Figure 8 shows a comparison of the Fourier spectra of the observed and synthetic S-waves; the Fourier spectra of the observed S-waveforms match well with those of the synthetic ones using the tuned model for the dominant components. The original and tuned structures at the TCG012 site are displayed in Fig. 9. In the figure, we can see that the first two layers in the original model are virtually absent in the tuned model; they are replaced with two thin layers based on the K-NET PS-logging data. Also depicted in Fig. 9 is the velocity structure at the TCG012 site by the National Research Institute for Earth Science and Disaster Prevention (NIED) model. The NIED velocity structure is not so different from the Yamanaka and Yamada model at the TCG012 site. Because the tuned structure differs greatly from the other two models, we are currently applying this tuning method at other sites and investigating the original and the tuned velocity models with other moderate earthquakes. In the next section, we discuss the above results, and limitations of the 1-D simulation for tuning the deep velocity structure in the case of the Kanto basin.

DISCUSSIONS AND CONCLUSIONS

In this study, we used the intermediate-depth moderate earthquakes for testing and tuning the deep velocity structure model of the north-west region of the Kanto basin reconstructed by Yamanaka and Yamada (2006). They derived the 3-D velocity structure of the Kanto basin based on the Rayleigh wave phase velocities at periods from 0.5 to 5 s deduced from microtremor array observations at more than 300 sites in the area. We applied 1-D method of waveform simulation and compared the observed and synthetic S-

waveforms applying several band-pass filters. Based on the waveform comparisons, we found that the Yamanaka and Yamada model (2006) reproduces well the observed S-waveforms at most sites located in the Tokyo metropolitan areas. However, it is found that the observed S-waveforms are overestimated at some sites in the northern and north-west region of the Kanto-basin suggesting further investigation of the velocity structures. We tuned the sedimentary velocity structure beneath the TCG012 site based on the 1-D simulation of long-period S-waves. It is found that the original and tuned structures have the similar depth to the seismic basement, but they differ largely in the layer thickness and S-wave velocities.

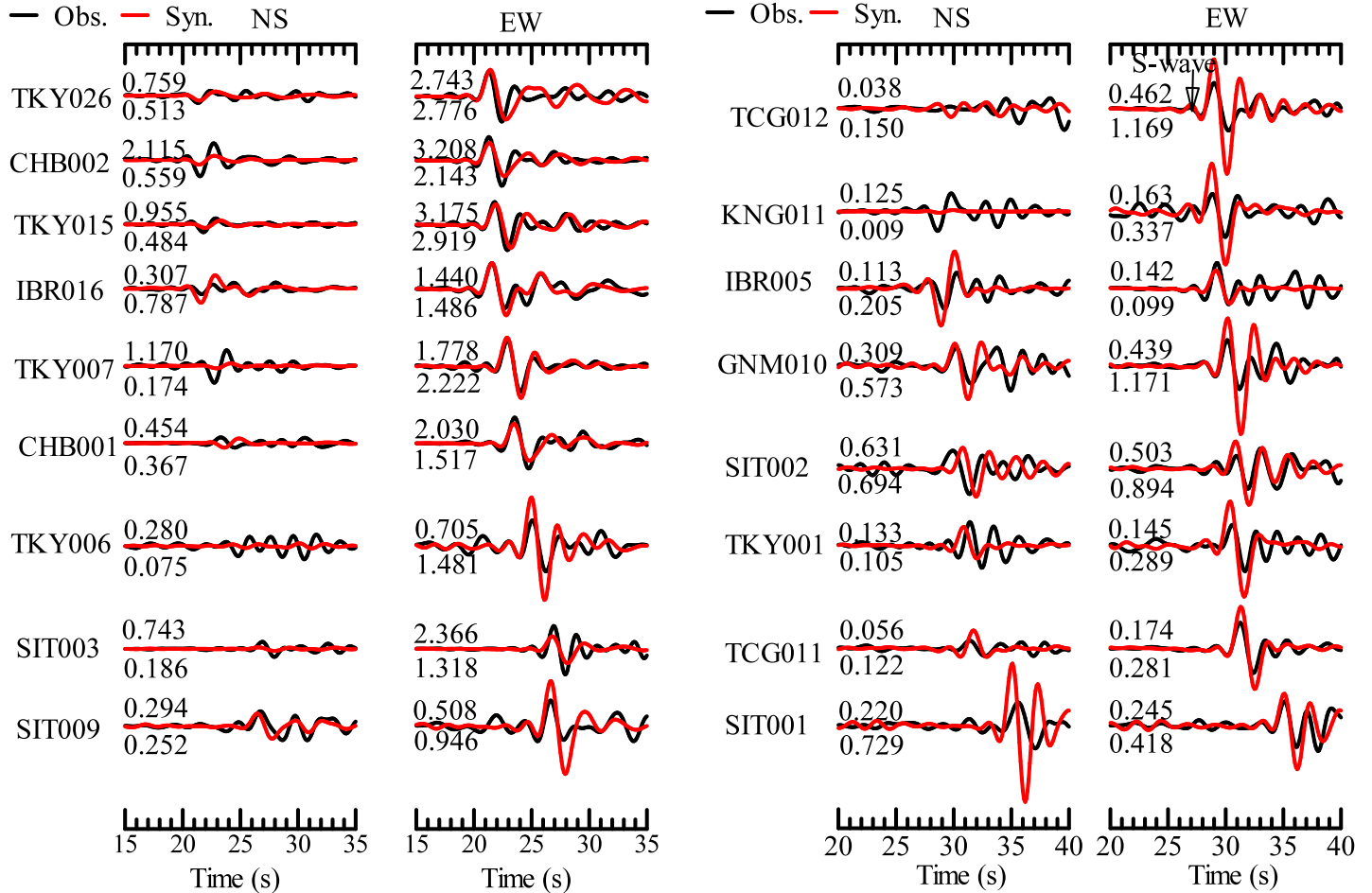


Fig. 6. Observed (black) and synthetic (red) velocity waveforms for the Mw 5.9, 2005 earthquake (Event No. 4, Table 2). The waveforms are bandpass filtered at 0.1-0.5 Hz; they are normalized by the maximum observed S-wave amplitude at each site. See captions in Fig. 3 for other details.

One of the difficulties in tuning the deep velocity structure based on the comparison of S-waveforms lies in the selection of time window for the waveform comparison. For the sites located on the basin-edges, the S-waveforms can be soon followed by or contaminated with basin surface waves. We, therefore, compared only the first cycle of the S-waveforms to avoid the effect of possible contamination. It is also difficult to derive accurate rise times with the 1-D method for the earthquakes that occur in a laterally highly heterogeneous upper mantle structures such as the ones beneath the Kanto basin, where the Pacific plate and the Philippine Sea plate subduct. The propagation path acts as a low pass filter by attenuating more rapidly the high frequency waves compared to the low frequency ones. Thus, due to the complex 3-D structure of the upper mantle beneath the Kanto basin, the path effect is not the same in every direction. In general, the path effect is considered to be less significant for long-period ground motion study. However, a more detailed analysis is needed to confirm the above assumption. On the other hand, the large difference of the S-wave amplitudes between the two horizontal components is mostly due to the radiation pattern of S-waves. The systematic overestimation of the S-wave amplitudes on the EW-components at western sites of the Kanto basin for the 2004 event is due to the poor resolution of the estimated radiation pattern of S-waves. Therefore, determination of accurate focal mechanism and rise time are

prerequisite for tuning the deep velocity structures using the S-waveforms only. However, it is not always possible to derive the well resolved rise time and focal mechanism for an earthquake. The comparison of the S-waveforms at the CHB002 site clearly illustrates the importance of finding the accurate focal mechanism acceptable to each site; the waveform fit for S-wave is poor at the CHB002 site for the 1997 event, while it is reasonable for the other events. Once the source parameters are well determined, we can reliably modify the 1-D velocity structure beneath the strong motion sites using the S-waveforms only. Therefore, we are currently investigating the original and the tuned velocity models with a number of moderate earthquakes for which a simple propagation path can be assumed. Probably the modified models can also be validated with the phase velocity data from the microtremor observations.

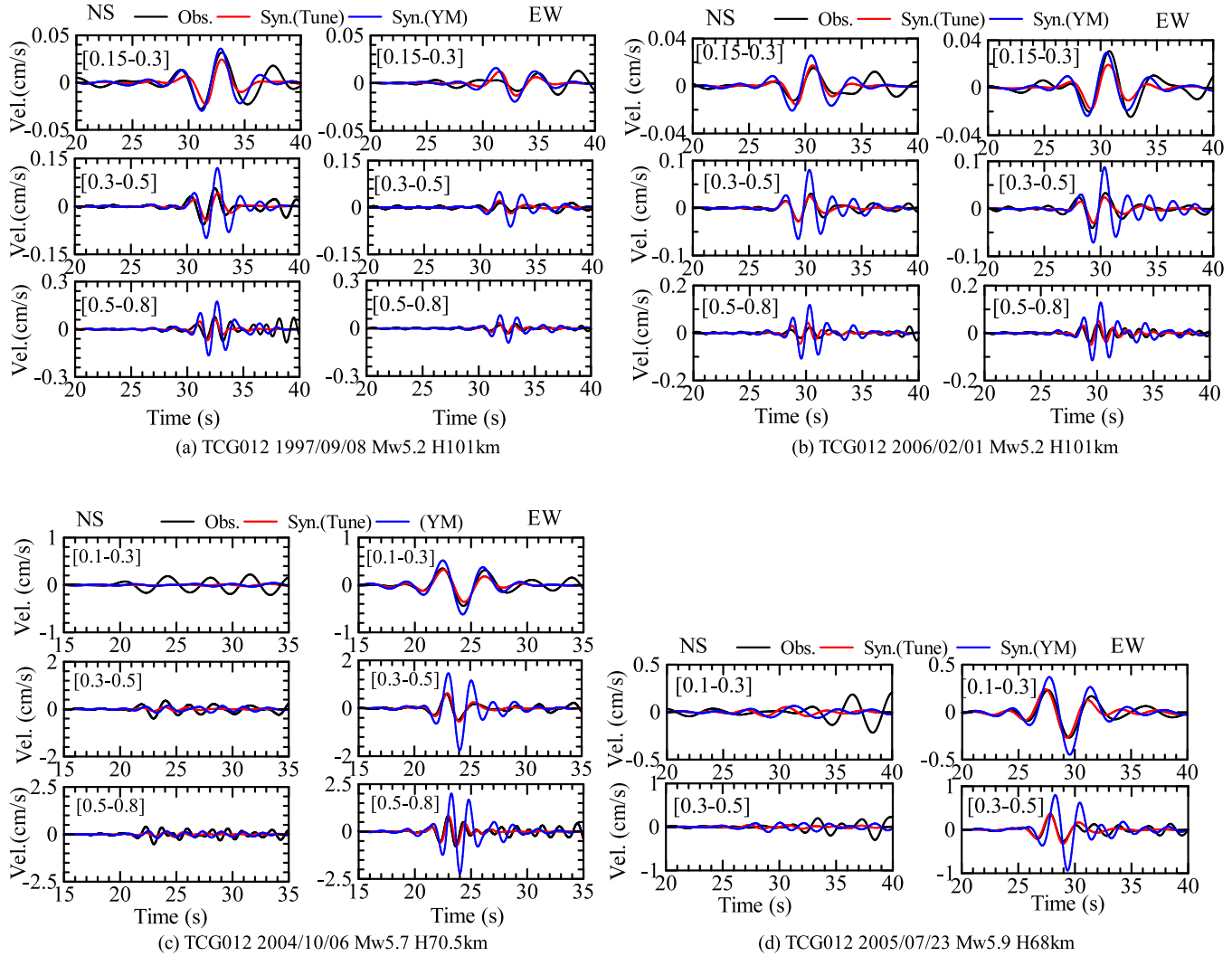


Fig. 7. Comparison between the observed and synthetic S-waveforms at the TCG012 site for the earthquakes (a) 1997/09/08 (Event 1, Table 2), (b) 2006/2/1 (Event 2, Table 2), (c) 2004/10/6 (Event 3, Table 2), and (d) 2005/7/23 (Event 4, Table 2). The pass band is shown in brackets in each panel. See Fig. 9 for the comparison of Fourier spectra.

ACKNOWLEDGEMENTS

We used the strong ground motion data from K-NET, earthquake source parameters from JMA, Global CMT database, and F-net. We used the underground velocity models reconstructed by Yamanaka and Yamada (2006). This research was partially supported by ‘Special project for earthquake disaster mitigation in Tokyo metropolitan area’ funded by the Ministry of Education, Culture, Sports, Science, and Technology, Japan.

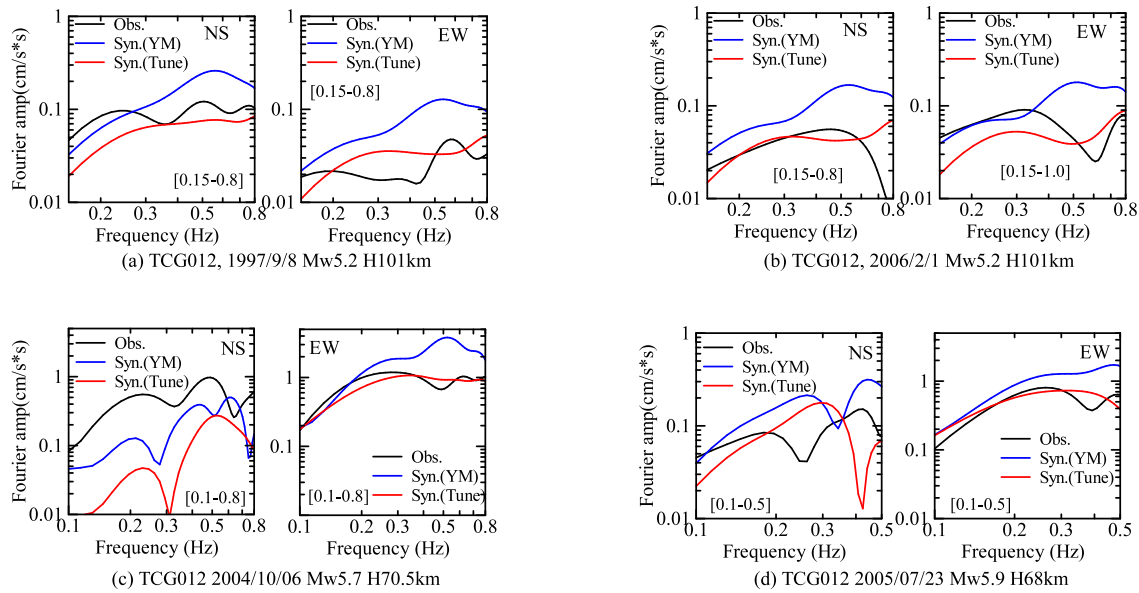


Fig. 8. Comparison between the observed and synthetic Fourier spectra of the S-waveforms depicted in Fig. 11. The Fourier spectra are derived for a time window of about 10 s having the first cycle S-wave at the centre of the time window.

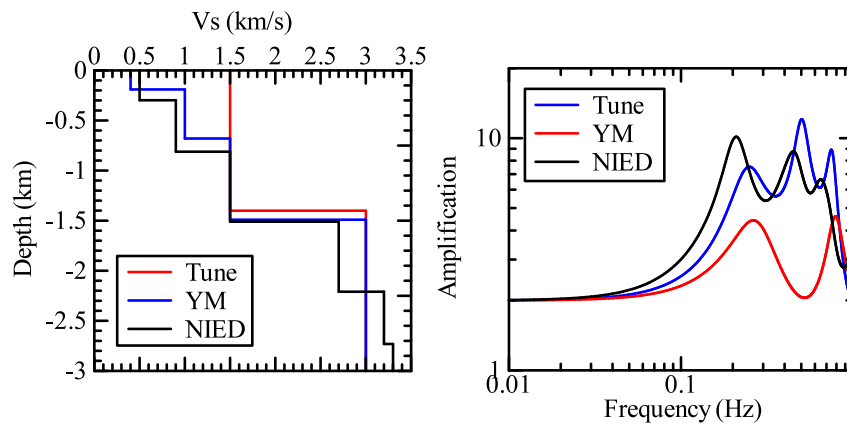


Fig. 9. Comparison of the S-wave velocity structures (left panel) and their site amplifications (right panel) at the TCG012 site for the tuned (Tune), Yamanaka and Yamada (2006) (YM), and NIED (2009) models.

REFERENCES

- Afnimar, K. Koketsu and M. Komazawa [2003], “3-D Structure of the Kanto basin, Japan from Joint Inversion of Refraction and Gravity Data”, *IUGG 2003 Scientific Program and Abstracts, SS04/07A/A03-002, B.487*.
- Ashiya, K., S. Asano, T. Yoshii, M. Ishida, and T. Nishiki [1987], “Simultaneous determination of the Three Dimensional Crustal Structure and Hypocenters beneath the Kanto-Tokai district, Japan”, *Tectonophysics*, Vol. 140, pp. 13-27.
- Bouchon, M. [1981], “A Simple Method to Calculate Green’s Functions for Elastic Layered Media”, *Bull. Seismol. Soc. Am.*, Vol. 71, pp. 959-971.
- Dhakal, Y. P., T. Sasatani, N. Takai [2009], “Tuning the deep velocity structure model by 1-D simulation of long-period S-waves”, *Proceedings of the 9th SEGJ International Symposium –Imaging and Interpretation–, Sapporo, Japan, 12-14 October, Paper ID 0112*.

- Dhakal, Y. P., T. Sasatani, N. Takai [2010], "Validation of the Deep Velocity Structure of the Tokachi Basin based on 3-D Simulation of Long-Period Ground Motions", *Pure and Applied Geophysics*, DOI 10.1007/s00024-010-0237-3.
- Ishida, M. [1992], "Geometry and Relative Motion of the Philippine Sea Plate and Pacific Plate beneath the Kanto-Tokai District, Japan", *J. Geophys. Res.*, Vol. 97, pp. 489-513.
- Iwaki, A. and T. Iwata [2009], "Validation of 3-D Basin Structure Models for Long-Period Ground Motion Simulation in the Osaka Basin, Western Japan", *J Seismol*, Vol. 12, 197-215.
- Koketsu, K. and S. Higashi [1992], "Three Dimensional Topography of Sediment/Basement Interface in Tokyo Metropolitan Area, Central Japan", *Bull. Seismol. Soc. Am.*, Vol. 82, pp. 2328-2349.
- Koketsu, K., H. Miyake, H. Fujiwara, and T. Hashimoto [2008], Progress towards a Japan Integrated Velocity Structure Model and Long-Period Ground Motion Hazard Map, *14th World Conf. on Earthq. Engg., China, Paper ID S10-038*.
- National Research Institute for Earth Science and Disaster Prevention (NIED) [2009] , <http://www.j-shis.bosai.go.jp/?lang=en>
- Rodgers, A., N. A. Petersson, S. Nilsson, B. Sjogreen, and K. McCandless [2008], "Broadband Waveform Modeling of Moderate Earthquakes in the San Francisco Bay Area and Preliminary Assessment of the USGS 3D Seismic Velocity Model", *Bull. Seismol. Soc. Am.*, Vol. 98, pp. 969-988.
- Suzuki, H. [1999], "Deep geological structure and seismic activity in the Tokyo Metropolitan area", *Journal Geography*, Vol. 108, No. 3, pp. 336-339 (in Japanese with English abstract).
- Suzuki, H. and H. Yamanaka [2008], "Estimation of S-wave velocity structure of deep sedimentary layers using a waveform inversion of S-wave in earthquake record", *Butsuri-Tansa*, Vol. 62, No. 2, pp. 261-275 (in Japanese with English abstract).
- Suzuki, H. and H. Yamanaka [2010], "Joint Inversion Using Earthquake Ground Motion Records and Microtremor Survey Data to S-wave Profile of Deep Sedimentary Layers", *Butsuri-Tansa*, Vol. 63, No. 3, pp. 215-227 (in Japanese with English abstract).
- Tanaka, Y., K. Koketsu, H. Miyake, T. Furumura, H. Sato, N. Hirata, H. Suzuki, and T. Masuda [2005], "The Daidaitoku Community Model of the velocity Structure beneath Tokyo Metropolitan Area", *2005 Joint Meeting for Earth and Planetary Science*, S079, p010.
- Yamanaka, H. and N. Yamada [2006], "Modeling 3D S-wave Velocity Structure of Kanto Basin for Estimation of Earthquake Ground Motion", *Butsuri-Tansa*, Vol. 59, No. 6, pp. 549-560 (in Japanese with English abstract).